Neutron-diffraction study of structural transition and magnetic order in orthorhombic and rhombohedral $La_{7/8}Sr_{1/8}Mn_{1-\gamma}O_{3+\delta}$

2007 J. Phys.: Condens. Matter 19 176226

(http://iopscience.iop.org/0953-8984/19/17/176226)

IOP PUBLISHING JOURNAL OF PHYSICS: CONDENSED MATTER

J. Phys.: Condens. Matter **19** (2007) 176226 (12pp) doi:10.1088/0953-8984/19/17/176226

Neutron-diffraction study of structural transition and magnetic order in orthorhombic and rhombohedral $La_{7/8}Sr_{1/8}Mn_{1-\gamma}O_{3+\delta}$

H F Li[1], Y Su[1], J Persson[1], P Meuffels[1], J M Walter[2], R Skowronek[2] and Th Brückel[1]

[1] Institut für Festkörperforschung, Forschungszentrum Jülich GmbH, D-52425 Jülich, Germany
[2] Neutron Diffraction Group of the Mineralogic-Petrological Institute of Bonn University, Research Center Jülich GmbH, MIN/ZFR, D-52425 Jülich, Germany

Received 28 January 2007, in final form 8 March 2007
Published 10 April 2007
Online at stacks.iop.org/JPhysCM/19/176226

Abstract

We report on a systematic neutron powder diffraction (NPD) study of polycrystalline $La_{7/8}Sr_{1/8}Mn_{1-\gamma}O_{3+\delta}$ compounds. We investigated the structural and magnetic phases and transitions in the temperature range between 10 and 900 K for two different samples: an Ar-annealed sample with an orthorhombic $Pbnm$ ($Z = 4$; O) structure at room temperature and an air-sintered sample with a rhombohedral $R\bar{3}c$ ($Z = 2$; R) structure at room temperature. At higher temperatures, above 400 K, both samples exhibit a rhombohedral structure. For the Ar-annealed sample, a Jahn–Teller (JT) transition occurs in the orthorhombic phase at about 298 K with very large variations in the Mn–O2′ and Mn–O2 bond lengths and Mn–O1–Mn bond angle on cooling from 298 to 180 K. For this sample the ferromagnetic moment at 10 K in the magnetic space group $Pb'n'm$ amounts to 3.22(5) μ_B/Mn. In contrast, the air-sintered sample undergoes on cooling a structural transition from rhombohedral (R) to orthorhombic (O) with a mixed phase of nearly equal R and O repartition at 120 K. Ferromagnetic order develops in this sample at about 240 K with a low-temperature moment of 3.35(4) μ_B/Mn at 10 K. The coherent JT distortion in its orthorhombic phase occurs below some 170 K. In addition, we have determined the coherent JT distortion parameter Δ, the tolerance factor t and the one-electron bandwidth W of the e_g-band.

(Some figures in this article are in colour only in the electronic version)

1. Introduction

The colossal magnetoresistance (CMR) manganites are technologically interesting materials, for example as cathode materials for solid fuel cells and new types of memory devices. However, their physical properties depend strongly on the preparation conditions. Therefore

a full understanding of the possible tuning of the physical properties in polycrystals, thin films and single crystals needs to be achieved before such applications become possible. The system $La_{1-x}Sr_xMnO_3$ has been widely investigated because of the very intriguing structural and physical phenomena that show large differences between polycrystals and single crystals; for example (i) structural evolutions versus temperature and Sr doping level, (ii) Curie temperature T_c and (iii) phase diagram including monotonic variations of the phase boundaries [1–8]. Only one report exists, where polycrystals show a similar phase diagram as the single crystals. However, for the polycrystalline samples, the transition-temperature ranges in resistivity (T) and magnetization (T) were much broader than those of the single crystals [9]. For nominal doping $x = 0.125$ at ambient conditions, the single crystal has an O structure [1, 2], but for polycrystals, depending on the preparation methods, different authors [3, 4] have reported O and R structures. Dutta *et al* [5] have reported the synthesis of nanoparticle $La_{0.875}Sr_{0.125}MnO_3$ samples with the R structure using a sol–gel method. For the same nominal Sr doping level, the structural and magnetic properties reported in the literature [1–5, 10, 11] differ substantially, strongly owing to the different preparation methods and synthesis conditions. Reentrant phase transitions from O ($c/\sqrt{2} < b \approx a$) to O′ ($c/\sqrt{2} < a < b$) at $T_{OO'} \approx 270$ K and subsequently to O″ ($c/\sqrt{2} < b < a$) at $T_{O'O''} \approx 150$ K in the $Pbnm$ symmetry were reported in a $La_{0.875}Sr_{0.125}MnO_3$ single crystal with $T_c \approx 180$ K [11]. The correlation between ferromagnetic spin orientation and coherent JT distortion was also studied [12]. In addition, the parent compound $LaMnO_3$ undergoes a structural transition at $T_{JT} \approx 750$ K [13], below which the JT distortion appears. On doping with Sr, the JT transition temperature is drastically reduced to $T_{JT} \approx 475$ K for a doping level of 0.1 [14]. However, the R structure, known as the high-temperature phase of nominal $La_{0.875}Sr_{0.125}MnO_3$, has received much less attention in the literature. Ersez [15] has investigated the magnetism of a polycrystalline $La_{0.875}Sr_{0.125}MnO_{3+\delta}$ with the R structure at room temperature and $T_c \approx 250$ K. He found no structural phase transition in the entire temperature range and a strong correlation of magnetic moment with unit cell dimension, but not with the Mn–O–Mn bond angle. However, the trace of Mn_3O_4 in his sample raises doubts on the stoichiometry. We know [16] that the structural and magnetic properties show huge responses on very small deviations from the nominal stoichiometry in this complex system.

In order to complete the structural study, solve issues in solid-state reactions and clarify the difference between polycrystalline and single-crystal samples of manganites, we decided to perform a detailed comparative study. We prepared two polycrystalline $La_{7/8}Sr_{1/8}Mn_{1-\gamma}O_{3+\delta}$ compounds with controlled nonstoichiometry through air sintering and Ar annealing in order to produce the O and R structures at room temperature. The R structure can be prepared for polycrystals, but has never been observed in $La_{7/8}Sr_{1/8}MnO_3$ single crystals at room temperature. The two samples undergo sharp ferromagnetic transitions [16] and the $T_c \approx 192$ K of the Ar annealed sample is very close to that of single crystals [11]. For both samples, we have found interesting magnetic properties and precisely determined the site occupancies through a combined refinement of room-temperature x-ray and NPD data [16]. In this paper we now report on the structural and magnetic properties and phase transitions from 10 to 900 K using NPD with the site occupancies of Mn and oxygen fixed to the room-temperature values [16]. This allows us to relate the magnetic order and properties to the crystal structure and thus resolve many ambiguities from the conflicting reports in the literature.

2. Experimental details

Polycrystals of $La_{0.875}Sr_{0.125}Mn_{1-\gamma}O_{3+\delta}$ were synthesized from stoichiometric mixtures of La_2O_3 (99.99%), MnO_2 (99.9%) and $SrCO_3$ (99.999%). After mixing and milling, the raw

materials were calcined twice at 1373 K for 12 h in air. The resultant powder was isostatically pressed into a cylindrical rod with a pressure of 54 MPa. After sintering twice at 1573 and 1623 K, respectively, for 18 h in air, half of the product was then pressed into a cylindrical rod that was annealed at 1273 K for 24 h in flowing gas of high-purity argon at 1 atm.

Powder samples for the structural study were obtained by carefully crushing the air-sintered and Ar-annealed rods. During the measurements, the samples were contained in tightly sealed vanadium cans. NPD data were collected in the angular range $2\theta = 0°$–$90°$ with a step size 0.1° at a wavelength of 1.0959 Å from 10 to 900 K on the powder diffractometer SV7-a at the FRJ-2 reactor in Jülich, Germany [17]. The data were analysed using the FullProf program [18].

3. Results

We have investigated the temperature variation of the crystal structures of two $La_{7/8}Sr_{1/8}Mn_{1-\gamma}O_{3+\delta}$ samples. The observed and calculated NPD patterns of Ar-annealed and air-sintered samples at selected temperatures are shown in figures 1(A) and (B), respectively. Observed patterns of the air-sintered sample in three Q regions at five selected temperatures are shown in the inset (a), where from the highest intensity to the lowest intensity the five patterns correspond to temperatures of 10, 65, 120, 180 and 270 K, respectively, with contrast effects to show the structural transition. Insets (b) and (c) show the refinement of only the nuclear structure for air-sintered (180 K) and Ar-annealed (10 K) samples, respectively, indicating the major contributions of magnetic scattering to the profiles. For the Ar-annealed sample, the nuclear and magnetic peak at $\sim$2.27 $Å^{-1}$, indexed as (200), (020) and (112) in $Pbnm$ symmetry, has a remaining nuclear contribution at 298 K as shown in the inset (d). This peak vanishes above 220 K in [4].

The refined structural parameters, calculated tolerance factor t and one-electron bandwidth W of the e_g-band are shown in figure 2. In order to compare the lattice parameter c with a and b for two samples, we plotted the equivalent c_{eq} for c in figures 2(a) and (b). Since for the air-sintered sample at 120 K a mixed O and R phase exists, the third set of parameters corresponding to the averaged values was calculated and plotted in addition. Thus one may observe three data points for one parameter at 120 K in figures 2(b), (d) and (h). The ideal cubic perovskite structure is usually distorted into a R or an O structure, when the tolerance factor $t = \langle \text{La(Sr)–O} \rangle \sqrt{2} \langle \text{Mn–O} \rangle$ is smaller than unity. For the Ar-annealed sample, t increases from 10 to 900 K (figure 2(c)), while for the air-sintered sample it stays nearly constant (figure 2(d)) at a larger value compared to the Ar-annealed sample in the entire temperature range. The temperature variation of the isotropic thermal parameters B of La(Sr), Mn and O atoms for the two samples are shown in figures 2(e) and (f), respectively. For the Ar-annealed sample, in the O structural region, the bond angle Mn–O2–Mn increases monotonically with temperature but is larger than Mn–O1–Mn. This leads to ⟨Mn–O–Mn⟩ remaining nearly constant below $\sim$180 K (close to T_c) and then increasing smoothly, but showing a large change in slope above $T_{OR} \approx 400$ K (figure 2(g)). By contrast, for the air-sintered sample (figure 2(h)), ⟨Mn–O–Mn⟩ increases smoothly from 300 to 900 K. Insets (c′) and (g′) schematically illustrate the MnO_6 octahedra in the O and R (hexagonal setting) structures, respectively, illustrating the relevant bond lengths. The bottom of figure 2(c) and inset (d′) show the individual Mn–O bond length for Ar-annealed and air-sintered samples in the O structural region, respectively. In that region Mn–O2 < Mn–O1 < Mn–O2′, while in the R region they are equal to each other. Large variations of Mn–O2′ and Mn–O2 in the temperature range 180 K < T < 298 K, with coincident changes of the lattice parameters, confirm that a very strong coherent JT distortion takes place for the Ar-annealed sample.

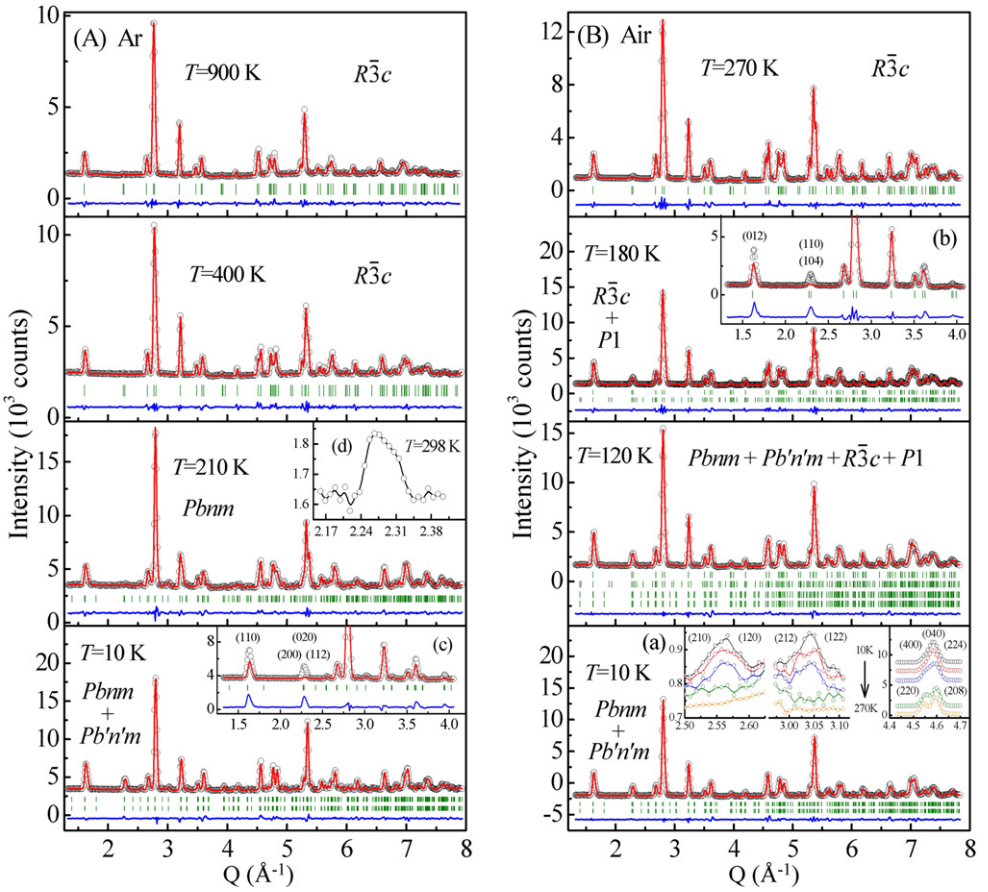

Figure 1. Observed (circles) and calculated (solid lines) patterns of (A) Ar-annealed and (B) air-sintered $La_{0.875}Sr_{0.125}Mn_{1-\gamma}O_{3+\delta}$ samples. The vertical bars mark the Bragg (top) and magnetic (bottom) peak positions. The line in the bottom of each diagram is the difference between the observed and calculated patterns. Inset (a) shows the observed patterns of the air-sintered sample in certain Q regions and from the highest to the lowest intensity the five patterns correspond to temperatures of 10, 65, 120, 180 and 270 K, respectively. Insets (b) and (c) show the refinement of only the nuclear structure for air-sintered ($T = 180$ K) and Ar-annealed ($T = 10$ K) samples, respectively. Inset (d) shows the existence of Bragg peaks indexed as (200), (020) and (112) in $Pbnm$ symmetry at 298 K for the Ar-annealed sample. For the air-sintered sample, a coexistence of magnetically ordered O with magnetically ordered R structures occurs.

Figures 3(a) and (b) schematically illustrate the Mn–O1–Mn, Mn–O2–Mn and Mn–O2′–Mn bond angles in the O structure and the Mn–O1–Mn angle in the R structure, respectively. For the O structure the bond angle Mn–O2–Mn is equal to Mn–O2′–Mn. Two kinds of distortion related to MnO_6 octahedra have been distinguished: (i) the cooperative rotation mainly corresponding to the Mn–O1–Mn bond angle; (ii) the JT distortion, inherent to high-spin ($S = 2$) Mn^{3+} ions, leading to large variations in bond lengths of Mn–O2 and Mn–O2′ lying in the acclivitous a–b plane of $Pbnm$ symmetry. Figure 4 shows the temperature dependences of the refined Mn moments and integrated intensities observed for Bragg reflections with magnetic intensity contributions for both samples. Insets (a) and (b) schematically illustrate the ordered moments for the Ar-annealed and air-sintered samples,

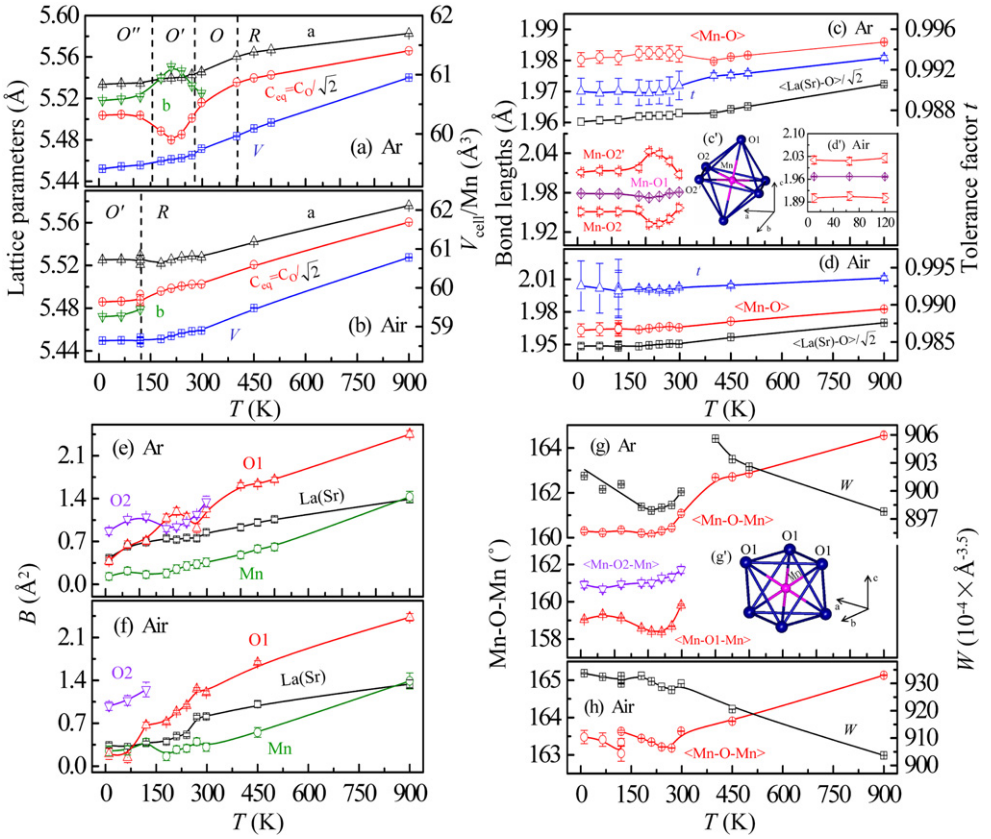

Figure 2. (a) and (b) Refined lattice parameters (left) and unit-cell volume V per Mn ion (right) versus temperature for (a) Ar-annealed and (b) air-sintered $La_{0.875}Sr_{0.125}Mn_{1-\gamma}O_{3+\delta}$ samples. The equivalent lattice parameter c_{eq} for the O and R structures is obtained by $c_{eq} = c_o/\sqrt{2}$ (O structure: $c_o = c_o$ and R structure: $a_h = (a_o - b_o - c_o)/2$, $b_h = b_o$, $c_h = 2a_o + c_o$ and $c_o = c_o$, so $9c_o{\cdot}c_o = c_h{\cdot}c_h + 12a_h{\cdot}a_h$. Subscripts h and o stand for hexagonal and orthorhombic, respectively). (c) and (d) Mean Mn–O and La(Sr)–O/$\sqrt{2}$ bond lengths (left) and tolerance factor t (right) versus temperature for (c) Ar-annealed and (d) air-sintered samples. (e) and (f) Temperature variation of the isotropic thermal parameters of La/Sr, Mn and O atoms for (e) Ar-annealed and (f) air-sintered samples. (g) and (h) Mean Mn–O–Mn bond angle (left) and one-electron bandwidth W of e_g-band (right) versus temperature for (g) Ar-annealed and (h) air-sintered samples. The bottoms of (c) and (g) show the individual Mn–O bond length and Mn–O–Mn bond angle of the Ar-annealed sample, respectively. Insets (c′) and (g′) show schematic illustrations of MnO_6 octahedra in the O and R structures, respectively. Inset (d′) shows the individual Mn–O bond length of the air-sintered sample in the O structure region.

respectively. The T_c determined from the temperature dependences of profiles of (110), (002) in the O structure and (012) in the R structure are consistent with the values reported by us earlier in [16]. Tables 1 and 2 show the refined atomic positions and reliability factors over the entire temperature range for Ar-annealed and air-sintered samples, respectively.

4. Discussion

Inset (a) of figure 1 in Q ranges 2.5–2.6 and 3.0–3.1 Å^{-1} shows the presence of Bragg reflections (210), (120) and (212), (122), respectively, at 10, 65 and 120 K. These peaks belong

Table 1. Refined structural parameters of Ar-annealed $La_{0.875}Sr_{0.125}Mn_{1-\gamma}O_{3+\delta}$ sample. The R structure was refined using the hexagonal (H) setting. Atomic positions for space group $R\bar{3}c$: La/Sr (0, 0, 1/4), Mn (0, 0, 0) and O1 (x, 0, 1/4); for $Pbnm$: La/Sr (x, y, 1/4), Mn (1/2, 0, 0), O1 (x, y, 1/4) and O2 (x, y, z). Numbers in parentheses are the estimated standard deviations (esds) of the last significant digit.

Synthesis	Ar-annealed											
T (K)	10	65	120	180	210	240	270	300	400	450	500	900
Crystal system	O	O	O	O	O	O	O	O	H	H	H	H
Space group	$Pbnm$	$Pbnm$	$Pbnm$	$Pbnm$	$Pbnm$	$Pbnm$	$Pbnm$	$Pbnm$	$R\bar{3}c$	$R\bar{3}c$	$R\bar{3}c$	$R\bar{3}c$
La/Sr:	4c	4c	4c	4c	4c	4c	4c	4c	6a	6a	6a	6a
x	−0.003(1)	0.001(1)	−0.002(1)	−0.004(1)	−0.005(1)	−0.004(1)	0.001(1)	0.0022(3)	0	0	0	0
y	0.0241(5)	0.0.235(5)	0.0240(5)	0.0246(6)	0.0226(6)	0.0219(6)	0.0203(6)	0.0212(4)	0	0	0	0
O1:	4c	4c	4c	4c	4c	4c	4c	4c	18e	18e	18e	18e
x	0.0647(8)	0.0638(8)	0.0644(8)	0.0656(8)	0.0662(7)	0.0664(7)	0.0657(8)	0.0622(9)	0.4464(3)	0.4465(3)	0.4470(3)	0.4522(3)
y	0.494(1)	0.493(1)	0.494(1)	0.491(1)	0.492(1)	0.493(1)	0.494(1)	0.4930(4)	0	0	0	0
O2:	8d	8d	8d	8d	8d	8d	8d	8d	—	—	—	—
x	0.728(1)	0.729(1)	0.729(1)	0.730(1)	0.734(1)	0.734(1)	0.732(1)	0.7305(9)	—	—	—	—
y	0.2796(7)	0.2794(7)	0.2791(7)	0.2788(7)	0.2803(6)	0.2797(6)	0.2791(7)	0.2763(8)	—	—	—	—
z	0.0334(4)	0.0344(4)	0.0338(4)	0.0341(3)	0.0352(3)	0.0347(3)	0.0340(4)	0.0332(4)	—	—	—	—
R_p (%)	3.81	3.63	3.73	3.68	3.73	3.65	3.61	2.88	3.39	3.67	3.44	3.28
R_{wp} (%)	5.34	4.93	5.13	4.91	4.84	4.77	4.85	3.91	4.58	4.86	4.57	4.43
χ^2	3.73	3.14	3.41	3.17	3.09	2.97	3.07	3.32	2.00	2.27	2.00	1.84
R_{mag} (%)	4.40	4.15	3.65	6.65	—	—	—	—	—	—	—	—

Table 2. Refined structural parameters of the air-sintered $La_{0.875}Sr_{0.125}Mn_{1-\gamma}O_{3+\delta}$ sample. The R structure was refined using the hexagonal (H) setting. Numbers in parentheses are the estimated standard deviations (esds) of the last significant digit.

Synthesis	Air-sintered										
T (K)	10	65	120		180	210	240	270	300	450	900
Crystal system	O	O	O	H	H	H	H	H	H	H	H
			50.8(14) wt%	49.2(14) wt%							
Space group	*Pbnm*	*Pbnm*	*Pbnm*	$R\bar{3}c$	$R\bar{3}c$	$R\bar{3}c$	$R\bar{3}c$	$R\bar{3}c$	$R\bar{3}c$	$R\bar{3}c$	$R\bar{3}c$
La/Sr:	4c	4c	4c	6a	6a	6a	6a	6a	6a	6a	6a
x	0.002(1)	0.002(1)	0.008(1)	0	0	0	0	0	0	0	0
y	0.010(1)	0.010(1)	0.011(2)	0	0	0	0	0	0	0	0
O1	4c	4c	4c	18e	18e	18e	18e	18e	18e	18e	18e
x	0.0605(8)	0.0605(7)	0.062(2)	0.4494(8)	0.4488(2)	0.4485(2)	0.4481(2)	0.4480(2)	0.4494(2)	0.4502(3)	0.4540(4)
y	0.499(2)	0.499(2)	0.501(3)	0	0	0	0	0	0	0	0
O2	8d	8d	8d	—	—	—	—	—	—	—	—
x	0.752(3)	0.751(3)	0.756(3)	—	—	—	—	—	—	—	—
y	0.263(1)	0.263(1)	0.260(2)	—	—	—	—	—	—	—	—
z	0.0325(4)	0.0327(4)	0.0340(6)	—	—	—	—	—	—	—	—
R_p (%)	3.76	3.84	2.97		3.98	3.42	3.15	3.11	2.72	2.94	3.61
R_{wp} (%)	5.36	5.32	4.11		5.25	4.63	4.28	4.25	3.64	4.00	4.99
χ^2	3.97	3.90	2.34		3.72	2.90	2.49	2.45	2.84	1.54	2.36
R_{mag} (%)	2.33	2.26	2.69	2.97	2.64	2.72	4.34	—	—	—	—

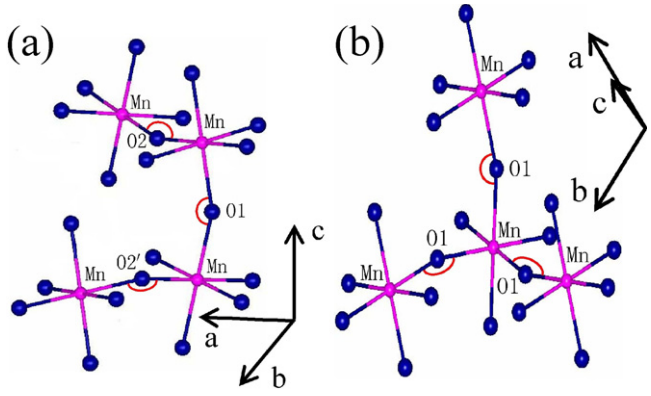

Figure 3. Schematic illustration of Mn–O1–Mn, Mn–O2–Mn and Mn–O2′–Mn (= Mn–O2–Mn) bond angles in the O structure of the Ar-annealed sample at 180 K (a) and Mn–O1–Mn in the R structure of the air-sintered sample at 180 K (b).

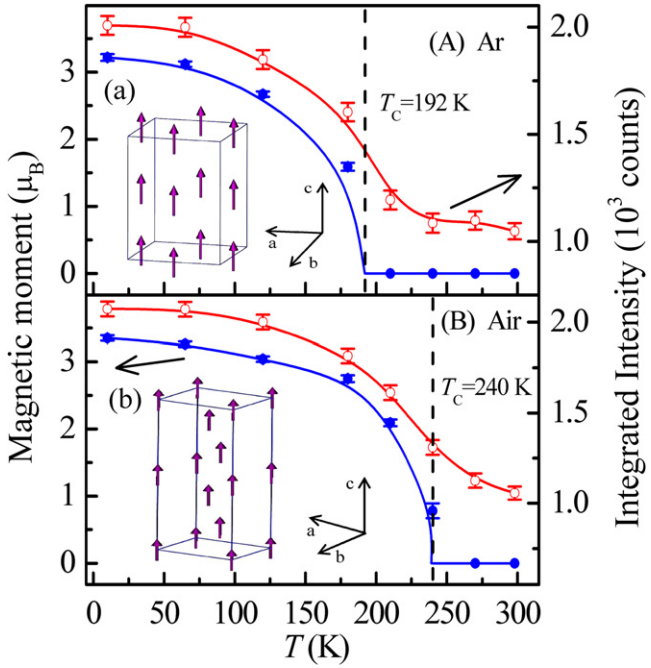

Figure 4. Refined Mn moment (left) and integrated intensity (right) observed at $Q = (110)$ and (002) of the O structure and $Q = (012)$ of the R structure versus temperature for (A) Ar-annealed and (B) air-sintered $La_{0.875}Sr_{0.125}Mn_{1-\gamma}O_{3+\delta}$ samples. Insets (a) and (b) schematically illustrate the ordered moments in ferromagnetic space groups of $Pb'n'm$ and $P1$, respectively. T_c is the onset temperature of ferromagnetic order based on SQUID measurements.

to the O structure and are absent at 180 and 270 K. In the Q range 4.4–4.7 $Å^{-1}$, one may observe a symmetric structural and magnetic peak indexed as (400), (040) and (224) in the O structure at 10 and 65 K. This peak splits into two peaks at 180 and 270 K, corresponding to nuclear as well as ferromagnetic reflections, which are indexed as (220) and (208) in the R structure. At 120 K, the shape of the peak becomes clearly asymmetric, indicating the existence of a mixed

R and O phase. The coalescence of (220) and (208) of the R setting in the O structure within the present resolution results not only from the structural changes, but also from the contribution of the magnetic peaks at 10, 65 and 120 K. We thus conclude that there is a structural transition from R to O between 180 and 65 K for the air-sintered sample, unlike [15]. In particular, at 120 K, a mixed R and O phase is observed with the refined weight percentage of 49.2(14) wt% and 50.8(14) wt%, respectively, which yields the smallest reliability factors (table 2). With a single phase, no satisfactory refinement can be achieved. By contrast, this transition from R to O happens in the Ar-annealed sample between 400 and 298 K (table 1). To summarize: for the Ar-annealed sample, we found the O structure between 10 and 298 K and the R structure between 400 and 900 K; for the air-sintered sample, we observe a pure O structure only below 65 K and the R structure between 180 and 900 K, while at 120 K a phase mixture was observed (table 2).

For the Ar-annealed sample (figure 2(a)), the lattice parameters very slowly increase from 10 to 120 K ($c_o/\sqrt{2} < b_o < a_o$; O″ phase). From 120 to 298 K, a rapid development of a large breathing-mode distortion corresponding to larger b_o than $c_o/\sqrt{2}$ is observed, whereas a_o continuously increases. At temperatures close to 180 and 270 K, the temperature variation curves of a_o and b_o cross one another ($c_o/\sqrt{2} < a_o < b_o$; O′ phase). From 298 to 400 K, as reported in $La_{1-x}Sr_xMnO_3$ with $x = 0.1$ [14], the lattice parameters should satisfy the relation $b_o < c_o/\sqrt{2} < a_o$, belonging to the so-called O phase. From 400 to 900 K, i.e. in the R region, a_h and c_{eq} increase much more rapidly than in the O region. We can conclude that the Ar-annealed sample follows the phase-transition sequence of the $La_{0.875}Sr_{0.125}MnO_3$ single crystal [11] O″–O′–O–R in the temperature range investigated. The differences between lattice parameters of O″ and O phases are by far smaller than those of O′ phase. We did not observe any splitting of Bragg peaks within our instrument resolution beyond the orthorhombic setting. For the air-sintered sample, we note nearly linear increases for a_h and c_{eq} in R region from 180 to 900 K, while in the O region from 10 to 120 K, a_o, $c_o/\sqrt{2}$ and b_o remain nearly constant (figure 2(b)). Moreover, from 10 to 120 K, the lattice parameters satisfy the relation $b_o < c_o/\sqrt{2} < a_o$, indicating that the air-sintered sample belongs to the O phase. Compared to the $x = 0.125$ single-crystal data [11], structural changes for our samples are less distinct. However, compared to [19], the Sr content in our samples is more stoichiometric, in agreement with the refined room-temperature data [16]. This indicates that one of the reasons for the differences in structural and physical properties between polycrystals and single crystals is the possible composition fluctuations.

The magnitude of the coherent Jahn–Teller distortion of MnO_6 octahedra can be evaluated by the following equation:

$$\Delta = \left(\frac{1}{6}\right) \sum_{n=1,6} \left[\frac{(d_n - \langle d \rangle)}{\langle d \rangle}\right]^2, \tag{4.1}$$

where $\langle d \rangle$ and d_n are the mean Mn–O bond length and the six Mn–O bond lengths along six different directions, respectively. The calculated values of Δ for both samples are shown in figure 5. For the Ar-annealed sample, Δ remains constant below 180 K and then drastically increases, showing a peak at ∼210 K. On further warming, it is strongly reduced, especially when T approaches $T_{JT} \approx 298$ K. Above 400 K, i.e. in the R region, Δ vanishes completely. For the air-sintered sample, Δ for the O structure below 120 K is comparable to that of the Ar-annealed sample at its maximal value at 210 K. In view of a large Δ below 120 K, resulting from big differences between three bond lengths (inset (d′) of figure 2) and suggesting strongly distorted MnO_6 octahedra, the O structure for the air-sintered sample is more like O′ phase than O phase. The coherent JT transition temperature is reduced to ∼170 K. For comparison, this kind of transition temperature of the parent compound $LaMnO_3$ is about 750 K [13]. On

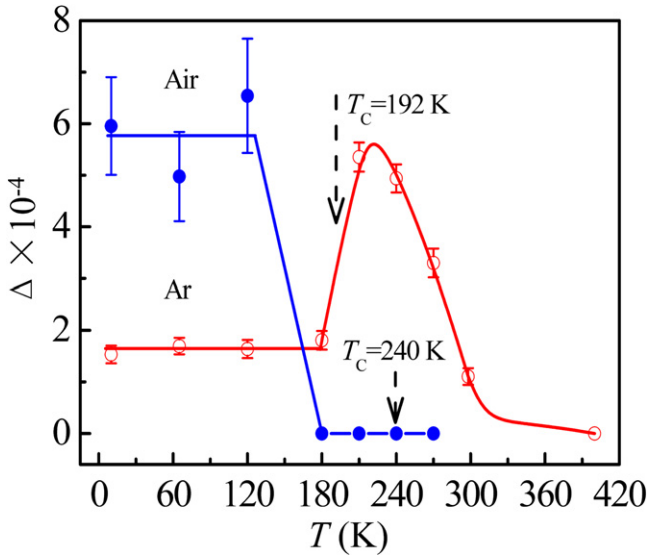

Figure 5. Temperature variation of the coherent JT distortion parameter Δ for Ar-annealed and air-sintered $La_{0.875}Sr_{0.125}Mn_{1-\gamma}O_{3+\delta}$ samples.

doping with Sr, T_{JT} is drastically reduced to $T_{JT} \approx 475$ K for a doping level of 0.1 [14]. Here, it is once more reduced to $T_{JT} \approx 298$ K for the Ar-annealed sample with Sr doping level 0.125, which is rather close to the reported value $T_{JT} \approx 270$ K for the single crystal [11]. Moreover, it is surprisingly decreased to ∼170 K for the air-sintered sample. It is worth mentioning that the coherent JT transition temperature strongly depends on the Mn^{3+} concentration, which can easily be changed by substitution and nonstoichiometry, e.g. Mn site vacancies and excess oxygen, etc. For the Ar-annealed sample, the onset of large coherent JT distortion leads to a phase transition from O to O′, accompanied by Mn^{3+} orbital order which is reflected by the bond lengths in the MnO_6 octahedra, i.e. the long Mn–O2′ and short Mn–O2 bonds lying in the acclivitous *a*–*b* plane and the medium Mn–O1 bonds almost along the *c* axis in *Pbnm* symmetry. In [19], this transition is considered as a disorder–order transition, during which the randomly disordered and highly distorted MnO_6 octahedra in the O phase form a long-range order in O′ phase. The ferromagnetic transition temperature ($T_c \approx 192$ K) is much smaller than $T_{RO} \approx 400$ K. Below 180 K, the long-range ferromagnetic order partly suppresses the coherent JT distortion to a smaller value, resulting in the O′ to O″ transition and the short-range order of highly distorted MnO_6 octahedra in the O″ phase, which indicates a strong coupling between the distortion of MnO_6 and the ferromagnetic order. The structural features of the O″ phase are similar to those of O phase, as is the JT distortion parameter Δ, whereas the magnetic states are severely different (O″ phase: ferromagnetic order; O phase: paramagnetic state). The air-sintered sample shows the effect of a ferromagnetic transition in the R structural region on the structural properties and the vestiges of a R–O structural transition in the ferromagnetic ordering state. The R–O structural transition is responsible for the appearance of a large coherent JT distortion, though in the whole O structural region the ferromagnetic order has already set in ($T_{RO} \approx 180$ K $< T_c \approx 240$ K). Thus there exist strong couplings between ferromagnetic ordering, coherent JT distortion and structural transition. For our two samples, the increase of T_c is accompanied by a shift of T_{RO} to lower temperatures, which seems to be universal for the lightly doped $La_{1-x}Sr_xMnO_3$ [19]. At T_{JT} and T_{OR} transition temperatures, the

unit-cell volume V per Mn ion displays anomalies in accordance with the case of $LaMnO_3$ [20], but unlike [5].

The effective electron transfer interaction between neighbouring Mn ions is governed by the superexchange process via O 2p states. The relative value of the one-electron bandwidth W of the e_g-band [21] can be estimated by

$$W \propto \frac{\cos\frac{1}{2}(\pi - \langle \text{Mn–O–Mn} \rangle)}{\langle \text{Mn–O} \rangle^{3.5}}. \tag{4.2}$$

Equation (4.2) shows that both the decrease of ⟨Mn–O–Mn⟩ and the increase of ⟨Mn–O⟩ result in the decrease of the W value. So W can be interpreted as a generalized parameter, combining the effects of ⟨Mn–O–Mn⟩ and ⟨Mn–O⟩. The calculated values of W for both samples are shown in figures 2(g) and (h). For the Ar-annealed sample, a band widening happens from $T_c \approx 192$ to 10 K, which is due to the small decrease of ⟨Mn–O⟩ bond length consistent with less insulating bonds as well as the slight increase of ⟨Mn–O–Mn⟩ bond angle, in agreement with a stronger orbital overlap of Mn–O bonds in O″ phase [19]. For the air-sintered sample, W decreases slowly in the entire temperature range. The decrease of ⟨Mn–O⟩ bond length and the increase of ⟨Mn–O–Mn⟩ bond angle from $T_c \approx 240$ to 120 K lead to a widening of the band, consistent with the creation of itinerant electrons and the development of metallic bonds in the ferromagnetic phase [19].

As to the magnetic structure, we did not detect any reflection forbidden by the crystal structure and pure ferromagnetism for both samples and thus there is no indication for canted ferromagnetism or antiferromagnetism. The ferromagnetic models having $Pb'n'm$ and $P1$ symmetries with ordered Mn moments along the c axis for the O and R structures, respectively, gave the best refinements. The theoretical saturation moments are 4 μ_B and 3 μ_B for Mn^{3+} and Mn^{4+} ions, respectively. Assuming quenched orbital angular momentum ($L = 0$; $J = S$), we calculated the effective saturation values of spin moments using Mn^{3+} and Mn^{4+} contents, which are evaluated from the refined site occupancies of room-temperature data based on the charge neutrality condition [16]. The calculated moments of 3.55(13) μ_B (Ar) and 3.60(13) μ_B (air) are in good agreement with the refined values of 3.22(5) μ_B (Ar) and 3.35(4) μ_B (air) for the two samples, respectively, considering all crude assumptions, e.g. purely integer valencies.

The ferromagnetic order below T_c is not changed by the different nuclear structures, O and R. On the other hand, the ferromagnetic ordering temperature is strongly dependent on these structural transitions resulting from different synthesis conditions, and decreases from 240 K (air) to 192 K (Ar). The detailed reasons for the remarkable decrease of T_c for the Ar-annealed sample in contrast with that of the air-sintered sample have been discussed in [16].

5. Conclusions

We have performed a comparative NPD investigation of the crystal and magnetic structures in the temperature range from 10 to 900 K for Ar-annealed and air-sintered $La_{7/8}Sr_{1/8}Mn_{1-\gamma}O_{3+\delta}$ samples with O and R structures at room temperature, respectively. The behaviour of Ar-annealed polycrystalline material is similar to the case of a single crystal. A series of structural transitions R–O–O′–O″ takes place successively with decreasing temperature from 900 to 10 K. The refined ferromagnetic moment is 3.22(5) μ_B/Mn at 10 K with spin orientation along the c axis in $Pbnm$ symmetry. The estimated JT transition temperature is drastically reduced to ∼298 K, compared with that of $LaMnO_3$ [13] ($T_{JT} \approx 750$ K) and that of $La_{0.9}Sr_{0.1}MnO_3$ ($T_{JT} \approx 475$ K) [14]. For the air-sintered sample, a structural transition from R to O has been observed to occur between 180 and 65 K. In particular, at 120 K, a mixed R (49.2(14) wt%) and O (50.8(14) wt%) phase exists. The structural transition temperature is severely decreased

compared to $T_{RO} \approx 400$ K for the Ar-annealed sample. The refined ferromagnetic moment is 3.35(4) μ_B/Mn at 10 K, being parallel to the c axis in $R\bar{3}c$ symmetry. Air sintering, leading to the R structure at room temperature, results in a remarkable decrease of the coherent JT transition temperature by ∼43% compared to that of the Ar-annealed sample, though no significant change in the magnitude of the coherent JT distortion parameter Δ was observed. Moreover, this study shows the existence of strong couplings between ferromagnetic ordering, JT distortion and structural transition. For the Ar-annealed sample, the appearance of ferromagnetic ordering below $T_c \approx 192$ K only partially suppresses the coherent JT distortion, but it is completely removed by the O–R structural transition for both samples. As already evidenced in our study [16], small differences in stoichiometry lead to largely different structural and physical behaviours in this system.

References

[1] Liu G L, Zhou J S and Goodenough J B 2001 *Phys. Rev.* B **64** 144414
[2] Su Y, Istomin K, Wermeille D, Fattah A, Foucart P, Meuffels P, Hupfeld D and Brückel Th 2004 *J. Magn. Magn. Mater.* **272** 291
[3] Jung J H, Kim K H, Lee H J, Ahn J S, Hur N J and Noh T W 1999 *Phys. Rev.* B **59** 3793
[4] Argyriou D N, Mitchell J F, Potter C D, Hinks D G, Jorgensen J D and Bader S D 1996 *Phys. Rev. Lett.* **76** 3826
[5] Dutta A, Gayathri N and Ranganathan R 2003 *Phys. Rev.* B **68** 054432
[6] Geck J, Wochner P, Kiele S, Klingeler R, Revcolevschi A, Zimmermann M V, Buechner B and Reutler P 2004 *New J. Phys.* **6** 152
[7] Paraskevopoulos M, Mayr F, Hartinger C, Pimenov A, Hemberger J, Lunkenheimer P, Loidl A, Mukhin A A, Ivanov V Yu and Balbashov A M 2000 *J. Magn. Magn. Mater.* **211** 118
[8] Kawano H, Kajimoto R, Kubota M and Yoshizawa H 1996 *Phys. Rev.* B **53** R14709
[9] Dabrowski B, Xiong X, Bukowski Z, Dybzinski R, Klamut P W, Siewenie J E, Chmaissem O, Shaffer J, Kimball C W, Jorgensen J D and Short S 1999 *Phys. Rev.* B **60** 7006
[10] Yamada Y, Suzuki J, Oikawa K, Katano S and Fernandez-Baca J A 2000 *Phys. Rev.* B **62** 11600
[11] Pinsard L, Rodriguez-Carvajal J, Moudden A H, Anane A, Revcolevschi A and Dupas C 1997 *Physica* B **234/236** 856
[12] Xiong X, Dabrowski B, Chmaissem O, Bukowski Z, Kolesnik S, Dybzinski R and Kimball C W 1999 *Phys. Rev.* B **60** 10186
[13] Rodriguez-Carvajal J, Hennion M, Moussa F and Moudden A H 1997 *Phys. Rev.* B **57** R3189
[14] Chatterji T, Ouladdiaf B, Mandal P, Bandyopadhyay B and Ghosh B 2002 *Phys. Rev.* B **66** 054403
[15] Ersez T 2002 *Mater. Lett.* **54** 211
[16] Li H F, Su Y, Persson J, Meuffels P, Walter J M, Skowronek R and Brückel Th 2007 *J. Phys.: Condens. Matter* **19** 016003
[17] Schaefer W, Jansen E, Skowronek R and Kirfel A 1997 *Physica* B **234–236** 1146
[18] Rodriguez-Carvajal J 1993 *Physica* B **192** 55
[19] Dabrowski B, Xiong X, Bukowski Z, Dybzinski R, Klamut P W, Siewenie J E, Chmaissem O, Shaffer J, Jorgensen J D and Short S 1999 *Phys. Rev.* B **60** 7006
[20] Maitra T, Thalmeier P and Chatterji T 2004 *Phys. Rev.* B **69** 132417
[21] Medarde M, Mesot J, Lacorre P, Rosenkranz S, Fischer P and Gobrecht K 1995 *Phys. Rev.* B **52** 9248